

Image Reconstruction from Incomplete Projection Data using Combined ART–CBP Algorithm

Suneet Singh, K. Muralidhar and P. Munshi

Indian Institute of Technology, Kanpur – 208 016

ABSTRACT

The present work is concerned with reconstructing cross-sections of composite structures when complete projection data is not available from the experiments. A novel approach combining the algebraic reconstruction technique (ART) and convolution back projection (CBP) algorithm has been developed for reconstruction with such data. The numerical results obtained reveal that a combination of ART and CBP is able to reconstruct cross-sections from incomplete data to an extent that is meaningful for non-destructive evaluation.

Keywords: Algebraic reconstruction technique, convolution back projection, combined ART-CBP, image reconstruction, non-destructive evaluation, computerised tomography

1. INTRODUCTION

Non-destructive evaluation (NDE) using computerised tomography¹ (CT) is an important methodology for inspection of material samples, including flaw detection in diverse applications, such as welded joints and solid rocket propellants. The utility of the convolution back projection (CBP) algorithm for CT in this class of problems has been reviewed by the authors². The success of CT as a non-destructive evaluation technique has prompted its usage for large objects as well.

It has been seen in applications that obtaining the required projection data for large objects may not be possible due to the limitation in the size of the scanners³. This is a major limitation when using the CBP algorithm. The input data for CT is obtained by scanning the object from various angles, starting from 0° and going up to 180°. The projection data is said to be complete only when

the entire object is scanned from every aspect of view angle. Commercial scanners in many situations cannot scan the full object, thereby record incomplete projection data. The present study explores the possibility of using incomplete data obtained from such scanners for image reconstruction.

During measurements related to NDE, the projection data is obtained for individual cross-sections to be reconstructed using x-ray and γ -ray sources. To gain experience with various algorithms, it is not however necessary to conduct physical experiments. Instead, the projection data can be calculated mathematically for geometrically simulated specimens. This approach has been adopted in the present study. The algebraic reconstruction technique (ART) family of algorithm has been used as a preconditioner to map the partial data to complete data, making it suitable for the CBP algorithm.

2. RECONSTRUCTION ALGORITHM

Tomographic inversion for reconstructing cross-sections using x-rays and γ -rays is based on the attenuation of the radiation intensity as it passes through the solid material being tested. The number of photon counts (N) after passing along a curve C in the material is given by

$$N = N_0 \exp \left[- \int_c \mu(r, \phi) dl \right] \quad (1)$$

where the integration is along the chord length of curve C , N_0 is the initial photon counts. In Eqn (1), μ is the attenuation coefficient that changes with position in a composite material. Since μ depends on the material distribution as well as the energy of radiation, a distribution of μ is a direct indicator of the material composition of the component being studied only for monoenergetic radiation sources. For the present study, the radiation source has been taken to be monoenergetic and the dependence of μ on the local material density alone has been included, ignoring the dependence on the wavelength. Equation (1) can be rewritten as

$$\ln \left(\frac{N_0}{N} \right) = \int_c \mu(r, \phi) dl = p(s, \theta) \quad (2)$$

The LHS of Eqn (2) is obtained from the measured data. Equation 2 is then to be viewed as the basis for calculating the density distribution in the object via the attenuation coefficient.

Tomographic algorithm used to solve Eqn (2) for $\mu(r, \phi)$ can be classified into the following three categories:

- (a) Transform methods, eg, CBP⁴ and direct Fourier techniques
- (b) ART⁵, additive and multiplicative
- (c) Optimisation techniques, eg, entropy and energy.

When the projection data available is large and complete, transform methods can be competently used. For incomplete data with a limited number of projections, ART has been recommended in the literature⁵. Transform methods are direct, whereas algorithms belonging to ART family are iterative.

3. ALGEBRAIC RECONSTRUCTION TECHNIQUE

The numerical solution of Eqn (2) using ART requires the discretisation of the cross-section of the object⁶. To formulate a discretised model, a Cartesian grid of square picture elements, called pixels, is introduced in the region to be reconstructed. These pixels are numbered following a regular fashion as shown in Fig. 1. The attenuation coefficient f_j is assumed to be constant throughout the j^{th} pixel. The source and the detector are considered as points, and the rays between these as lines. During measurement, the full cross-section is scanned by moving the source-detector pair by a translator mechanism. The length of intersection of the i^{th} ray and j^{th} pixel, denoted by w_{ij} represents the contribution of j^{th} pixel to the total attenuation along the i^{th} ray. The indices i and j vary as $i = 1, 2, \dots, M$ and $j = 1, 2, \dots, N$.

The attenuation of the i^{th} ray within the object is denoted by ϕ_i and represents the line integral of the attenuation function along the path of the ray. Measurements lead to the data in terms of ϕ_i . In the discretised model, the line integral is represented by the sum

$$\phi_i = \sum_{j=1}^N f_j w_{ij} \quad i = 1, 2, \dots, M \quad (3)$$

Thus, the discretised model may be described by a system of linear equations. In matrix notation

$$[w_{ij}] \{f_j\} = \{\phi_i\} \quad (4)$$

The problem now reduces to inversion of the rectangular matrix $[W_{ij}]$, and subsequent calculation of the field values f_j at the pixel locations.

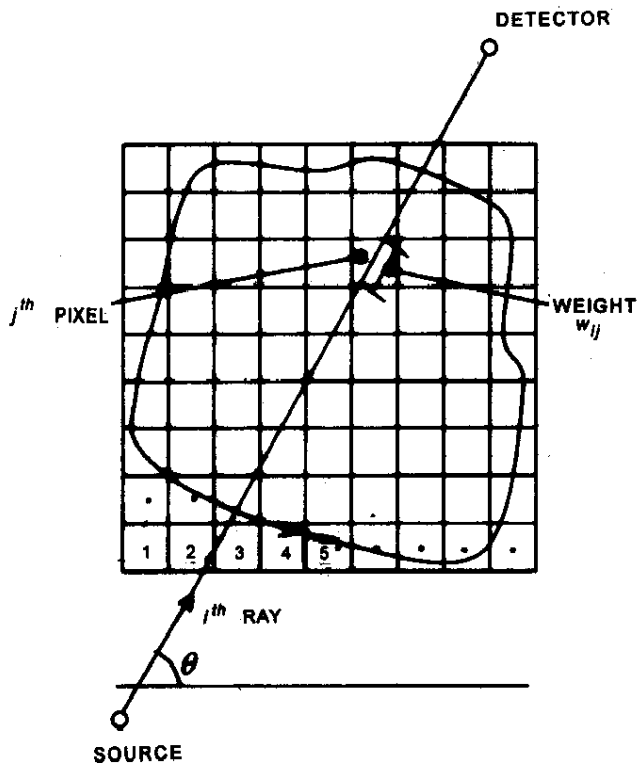


Figure 1. Discretisation of an object cross-section into an array of pixels.

The algorithm based on the ART family, which is used to invert the matrix, is iterative and consists necessarily of four major steps: (i) assumption of the test field, (ii) calculation of the pixel-level correction, (iii) application of correction, and (iv) test for convergence.

Let $\phi_{i\theta}$ be the projection due to i_0^{th} ray with the angle of irradiation θ and f_j be the initial guess of the field value. An intermediate quantity $\tilde{\phi}_{i\theta}$ is computed using the guessed field as

$$\tilde{\phi}_{i\theta} = \sum_{j=1}^N w_{i_0,j} f_j \quad i_0 = 1, 2, \dots, M_\theta \quad (5)$$

where i_0 denotes the i^{th} ray of the irradiation specified by angle θ and $1 \leq i_0 \leq M_\theta$. The subsequent calculation steps are as follows:

- For each angle of radiation θ

Step 1. Calculate the correction term K for each ray

Step 2. Apply the correction for each cell j of the test field if $w_{i_0,j}$ is non-zero in the form

$$f_j^{\text{new}} = f_j^{\text{old}} + K \quad (\text{additive ART})$$

$$f_j^{\text{new}} = f_j^{\text{old}} \times K \quad (\text{multiplicative ART})$$

Step 3. Repeat step 2 for all the rays of the irradiation with angle θ

- Update the approximate projection using Eqn (5)
- Repeat the above procedure for all the angles of irradiation. This completes the k^{th} global iteration
- Iterate until

$$\frac{f^{\text{new}} - f^{\text{old}}}{f^{\text{old}}} \times 100 \leq e$$

where e is the stopping criterion, say 0.01 per cent.

The correction term K is different for each class of the ART algorithm. The correction term⁷ for additive ART is

$$K = \lambda \frac{\phi_{i\theta} - \tilde{\phi}_{i\theta}}{\sum_{j=1}^N w_{i_0,j}} \quad (6)$$

where λ is the relaxation factor.

In multiplicative ART (MART), the correction term⁸ is multiplicative and is given as

$$K = 1 - \lambda \frac{w_{ij}}{W_{\max}} \left(1 - \frac{\phi_i}{\tilde{\phi}_i}\right) \quad \text{if } \tilde{\phi}_i \neq 0 \text{ and } w_{ij} \neq 0;$$

else

$$K = 1 \quad (7)$$

Here, λ is once again a suitable relaxation factor having a value between zero and two. In practice, the relaxation factor in Eqns (6) and (7) is kept at values below unity for achieving good contrast.

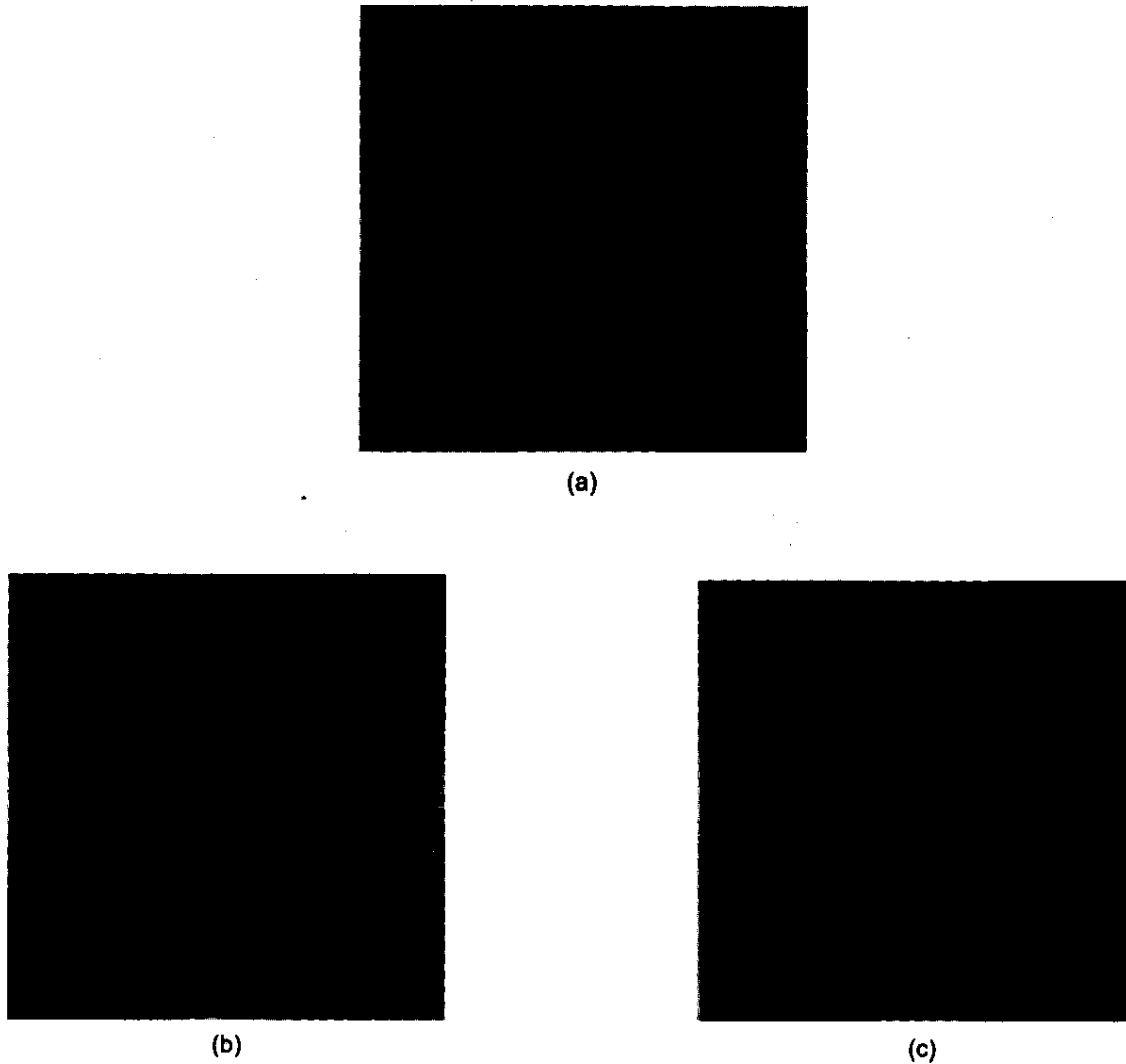


Figure 2. Original as well as reconstructed cross-sections using additive ART and MART algorithms with 64 rays \times 64 views: (a) original object on 64×64 grid, (b) reconstructed image using additive ART, $\lambda = 0.9$, ART iterations = 80, CPU time = 1.5 min, and (c) reconstructed image using MART, $\lambda = 0.9$, MART iterations = 750, CPU time = 14 min.

4. RECONSTRUCTION WITH COMPLETE DATA USING ART & MART

To check the intrinsic correctness of the ART family of algorithms, a simulated object has been reconstructed with complete data. Figure 2 shows the reconstruction of the object with a projection data set of 64 rays and 64 views. Figure 3 shows a similar result with a projection dataset of 256 rays and 256 views. The original object cross-section on a 64×64 and a 256×256 grid has been included for comparison with the reconstructions.

Examining Figs 2 and 3, the reconstructed images are seen to be quite similar to the simulated object. The pixel-level errors have been calculated to be within reasonable limits for both ART and MART. It is worth noting that the reconstruction using ART and MART preserves small as well as global features in the simulated object. The present quality of reconstructions favourably compares with the reconstructions using the CBP algorithm². Comparing Fig. 2 with Fig. 3, it can be seen that the quality of the reconstructed image improves significantly as the number of views and rays are increased.

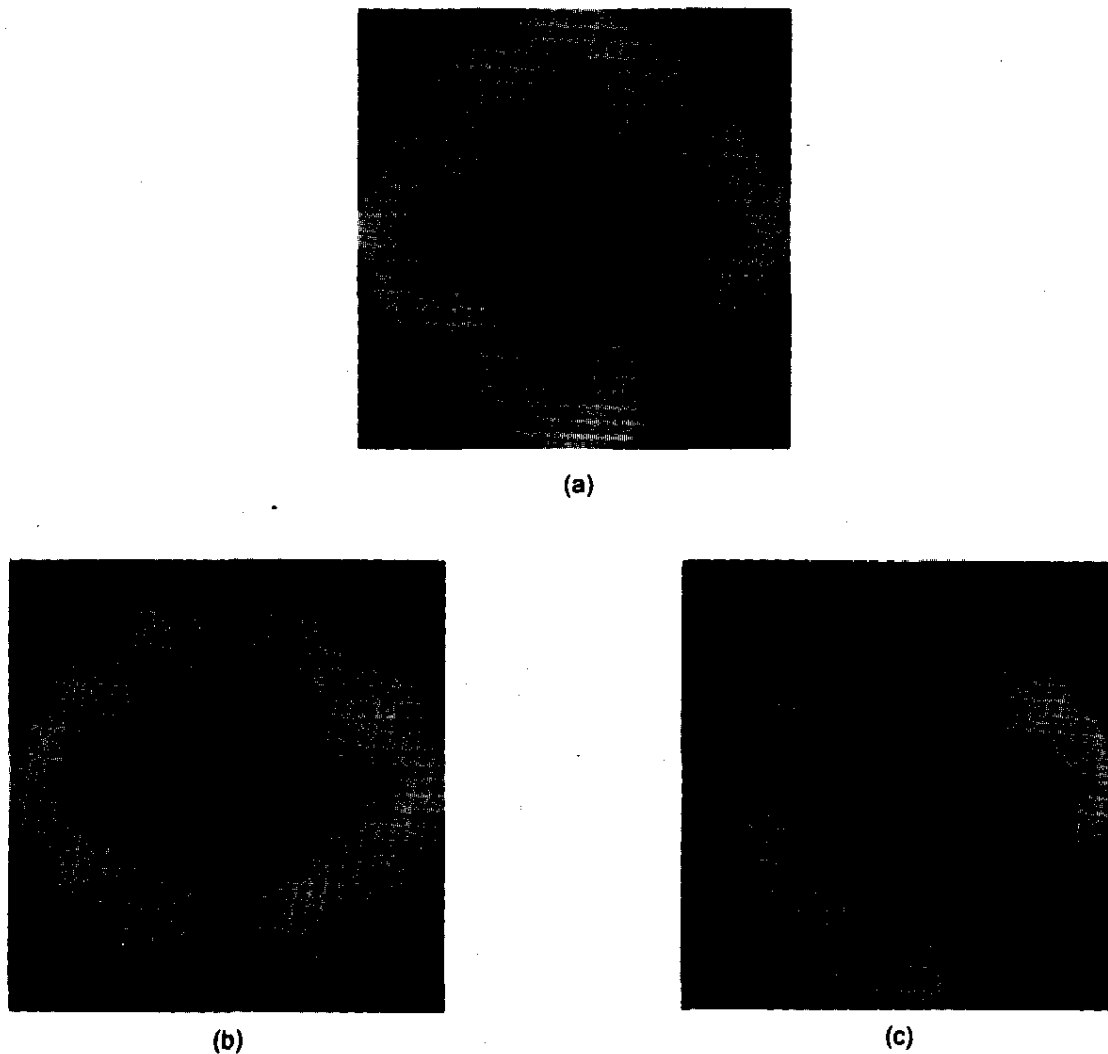


Figure 3. Original as well as reconstructed cross-sections using additive ART and MART algorithms with 256 rays \times 256 views: (a) original object on 256 \times 256 grid, (b) reconstructed image using additive ART, $\lambda = 0.9$, ART iterations = 18, CPU time = 210 min, (c) reconstructed image using MART, $\lambda = 0.9$, MART iterations = 120, CPU time = 1560 min.

An assessment of the algorithm in terms of the absolute error in the object reconstruction leads to the following conclusions:

- Errors in MART are less and evenly distributed whereas those in ART are more but localised.
- Increasing the number of rays and views, predictions of ART appear to be superior to MART.
- The CPU time requirement of ART is consistently lesser than that of MART.
- Predictions of MART are superior from a non-destructive evaluation perspective when the number of views are restricted.

An additional observation applicable to both algorithms is that the ART family is capable of treating partial projection data and converges to an intermediate solution.

5. COMBINED ART-CBP ALGORITHM FOR INCOMPLETE DATA

As stated earlier, large-sized objects cannot be fully scanned by commercially available

source-detector systems. This leads to a situation wherein the projection data is incomplete, making an algorithm, such as CBP ineffective. A modified approach to circumvent this difficulty has been developed. The data required to test the proposed algorithm has also been numerically determined. Though the data is incomplete wrt a given view angle, it is important to ascertain that all the projections together carry the total information about the object.

The algorithm developed in the present study for reconstruction of image cross-sections from an incomplete set of projection data is as follows:

- Step 1.* Reconstruct the object with the incomplete projection data using ART
- Step 2.* Compute the complete projection data numerically for the image reconstructed in *step 1*
- Step 3.* Combine the original (partial) dataset with that of *step 2*
- Step 4.* Reconstruct the object with the complete projection data now available from *step 3* using CBP
- Step 5.* Repeat *steps 2* and *3*
- Step 6.* Reconstruct the object with the projection data of *step 5* using ART. This completes an iteration
- Step 7.* Repeat *steps* from *2* to *6* until the difference in the images of two successive iterations in terms of pixel values is negligible.

6. RESULTS OF PROPOSED ALGORITHM

The star-shaped object considered in Figs 2 and 3 has been taken for analysis once again. Though the projection data is incomplete, the essential symmetricity of the object has been retained. As before, projections have been computed numerically. Experiences with both the additive ART and MART have been reported. Figs 4 to 7 deal with 75 per cent partial data, while Figs 8 and 9 are for 50 per cent data. The CPU time referred in Figs 2 to 9 were obtained on an

intel P-II computer, 400 MHz clock speed, with 128 Mbyte RAM.

Figures 4 and 5 show reconstruction using ART and MART, respectively with 64 rays and 64 views. Figures 6 and 7 show reconstruction with ART and MART, respectively with 256 rays and 256 views. Each of the Figs 4 to 7 shows reconstruction with projection data obtained by scanning 75 per cent of the object. For reconstructions shown in Figs 8 and 9, only 50 per cent of the object has been scanned. The projection data used for Fig. 8 comprises 64 rays and 64 views, while that for Fig. 9 has 256 rays and 256 views. Both the original image and the image reconstructed with incomplete projection data have been included in each of the figures. The intermediate images obtained using CBP and the images obtained after each iteration are also included for comparison. It should be noted that the original image referred here pertains to its representation on the appropriate grid, namely, 64×64 or 256×256 . Errors are to be referred to the discretised original image during the assessment of the algorithm.

The first reconstruction obtained with ART/MART with incomplete projection data, shows the presence of unrealistic artifacts. Though the dominant features are seen to be captured, the quality of the image is poor and the outer boundary is not clearly discerned. When the first iteration is complete, the projection data set is complete and significant improvement in the images is obtained. The outer circular boundary reappears and the artifacts introduced at the first step of first iteration diminish in strength. With increasing iterations, the reconstructed image approaches the original image. These trends can be seen with ART as well as MART algorithm. The trends are similar for the projection data with 64 rays \times 64 views and projection data with 256 rays \times 256 views. The errors in MART are marginally less when the number of views are lesser, compared to ART. With 256 views, however, the object is fully resolved at local and global scales and the errors in the simulation are quite lesser. The difference in CPU time of each algorithm is an important factor.

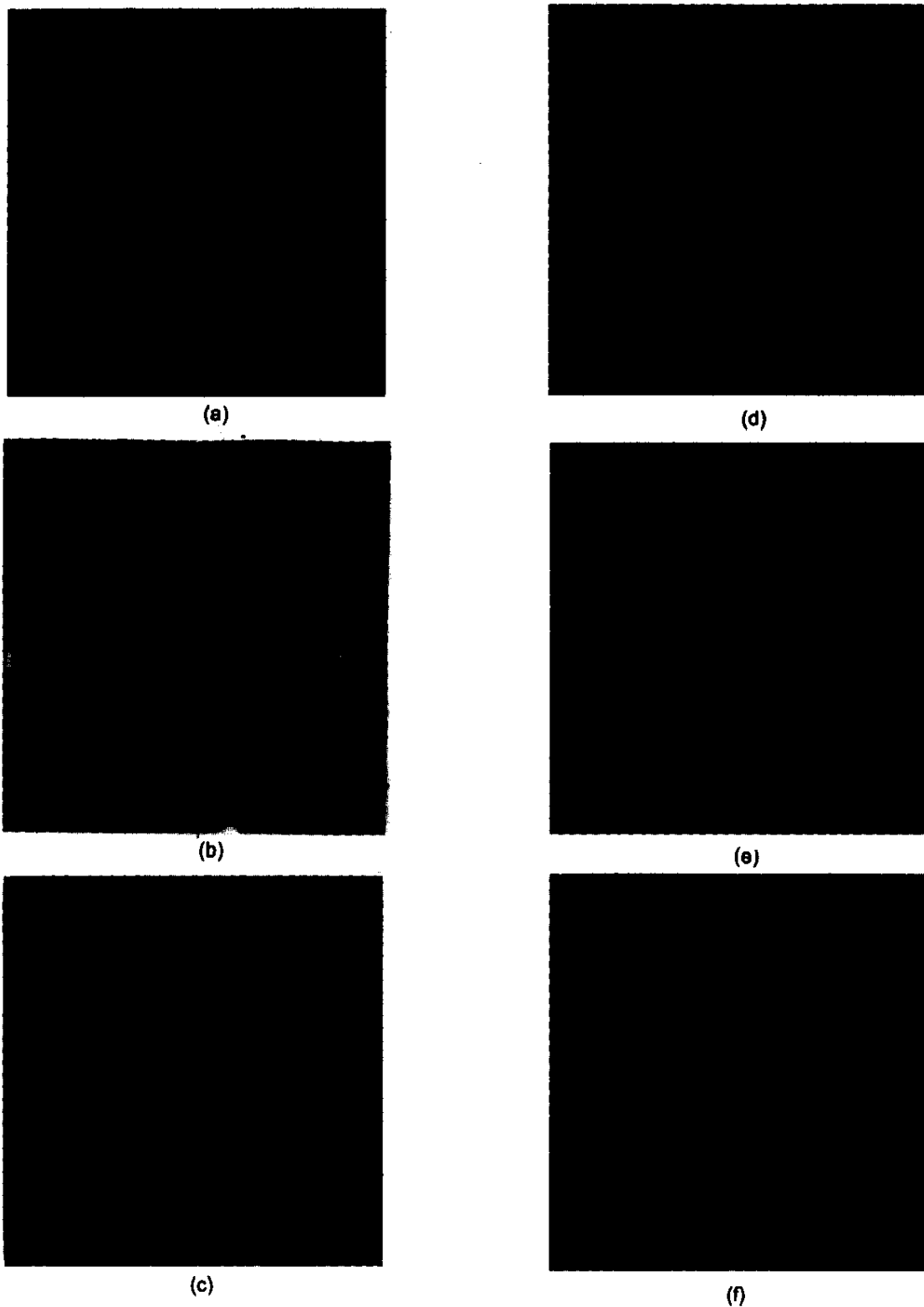


Figure 4. Combined ART-CBP algorithm results with 75 per cent complete symmetric data for 64 rays \times 64 views: (a) original object on 64 \times 64 grid, (b) reconstructed image using CBP, (c) reconstructed image using CBP, (d) reconstructed image with partial data using ART, $\lambda = 0.9$, ART iterations = 80, CPU time = 1.5 min, (e) image after first iteration, $\lambda = 0.9$, ART iterations = 120, CPU time = 2 min, and (f) image after second iteration, $\lambda = 0.9$, ART iterations = 120, CPU time = 2 min.

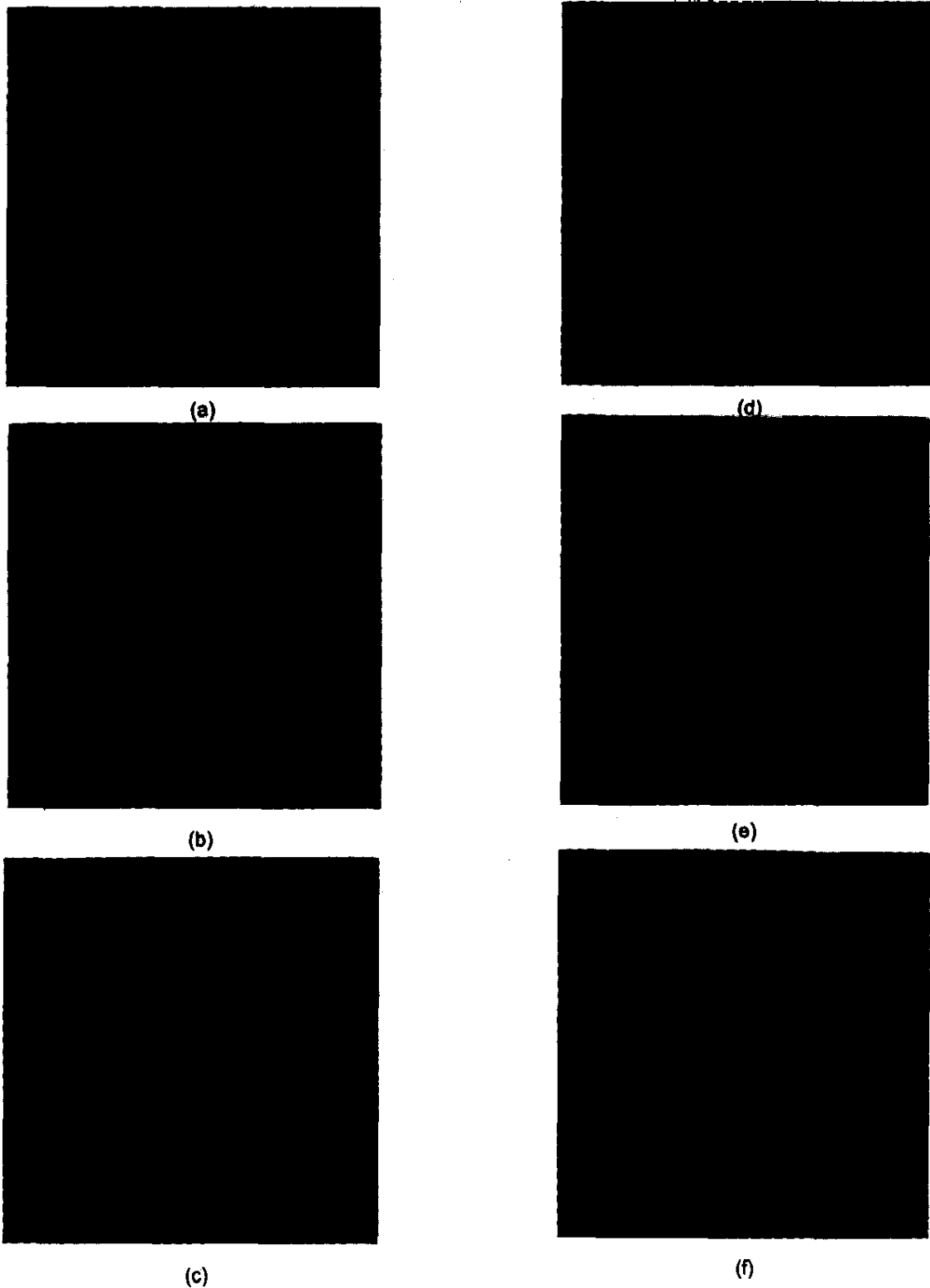


Figure 5. Combined ART-CBP algorithm results with 75 per cent complete symmetric data for 256 rays \times 256 views: (a) original object on 256 \times 256 grid, (b) reconstructed image using CBP, (c) reconstructed image using CBP, (d) reconstructed image with partial data using ART, $\lambda = 0.9$, ART iterations = 17, CPU time = 210 min, (e) image after first iteration, $\lambda = 0.9$, ART iterations = 20, CPU time = 240 min, and (f) image after second iteration, $\lambda = 0.9$, ART iterations = 20, CPU time = 240 min.

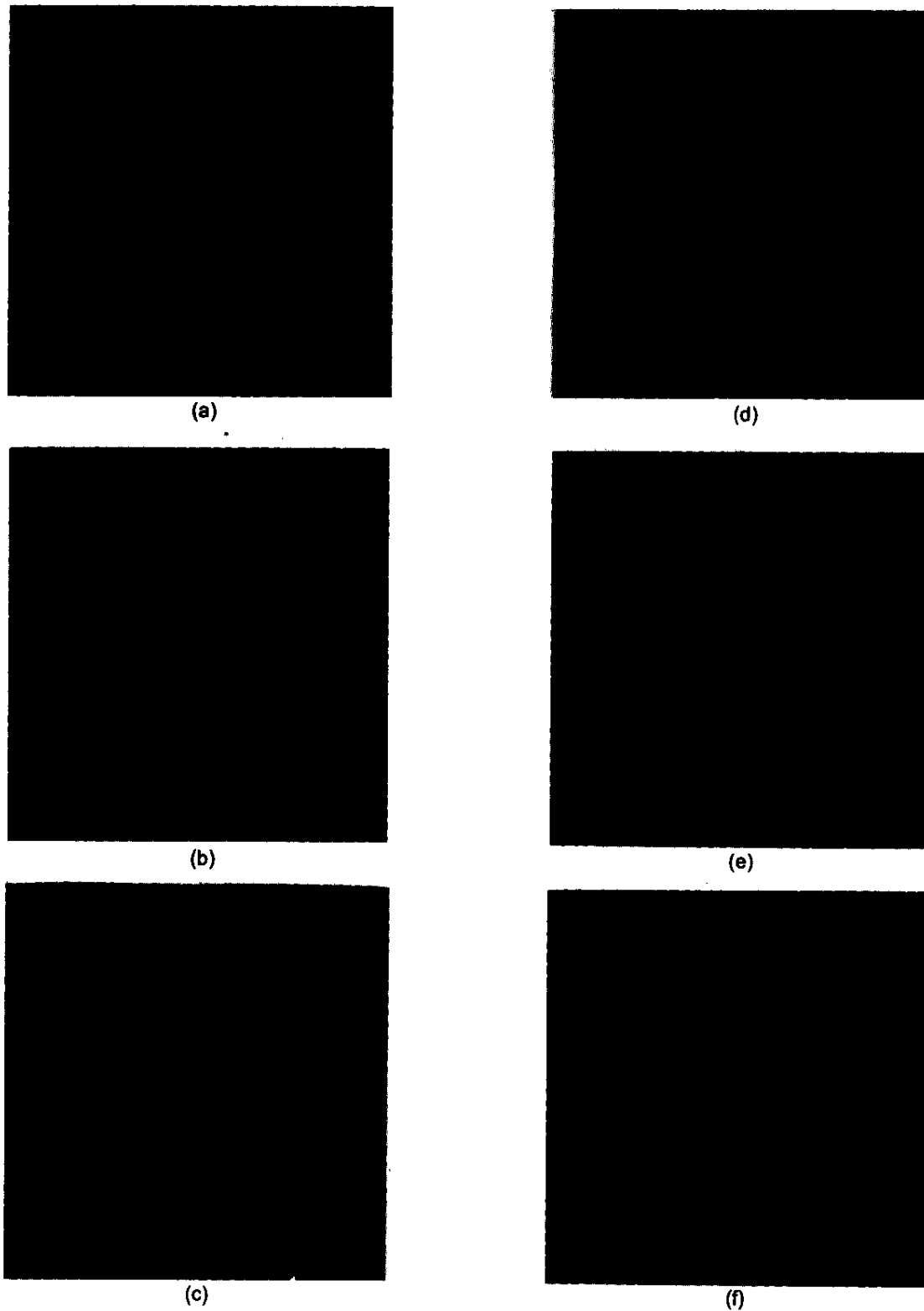


Figure 6. Combined CBP-MART algorithm results with 75 per cent complete symmetric data for 64 rays \times 64 views: (a) original object on 64 \times 64 grid, (b) reconstructed image using CBP, (c) reconstructed image using CBP, (d) reconstructed image with partial data using MART, $\lambda = 0.9$, MART iterations = 830, CPU time = 14 min, (e) image after first iteration, $\lambda = 0.9$, MART iterations = 920, CPU time = 16 min, and (f) image after second iteration, $\lambda = 0.9$, MART iterations = 920, CPU time = 16 min.

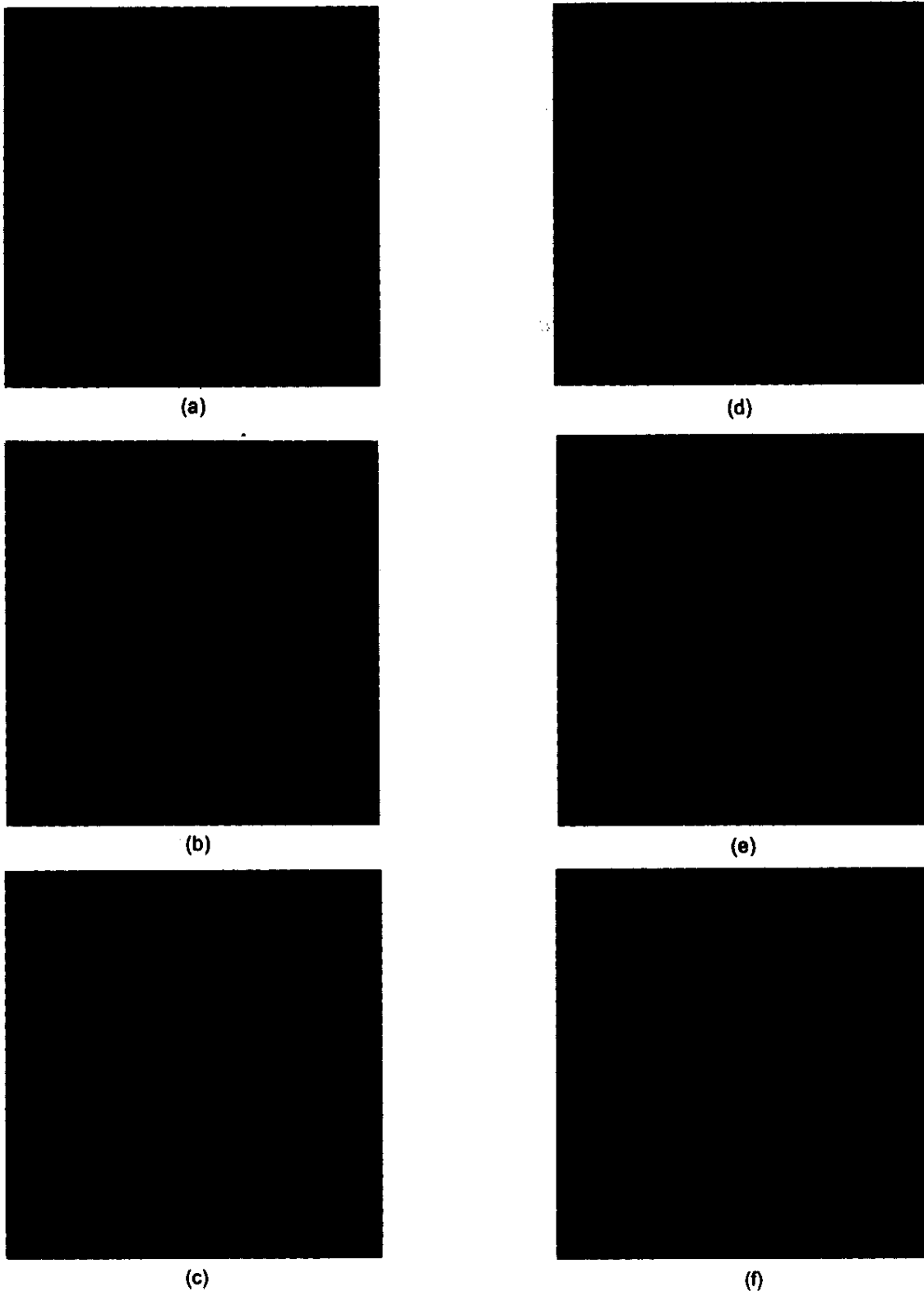


Figure 7. Combined MART-CBP algorithm results with 75 per cent complete symmetric data for 256 rays \times 256 views: (a) original object on 256 \times 256 grid, (b) reconstructed image using CBP, (c) reconstructed image using CBP, (d) reconstructed image with partial data using MART, $\lambda = 0.9$, MART iterations = 130, CPU time = 1560 min, (e) image after first iteration, $\lambda = 0.9$, MART iterations = 135, CPU time = 1570 min, and (f) image after second iteration, $\lambda = 0.9$, MART iterations = 135, CPU time = 1570 min.

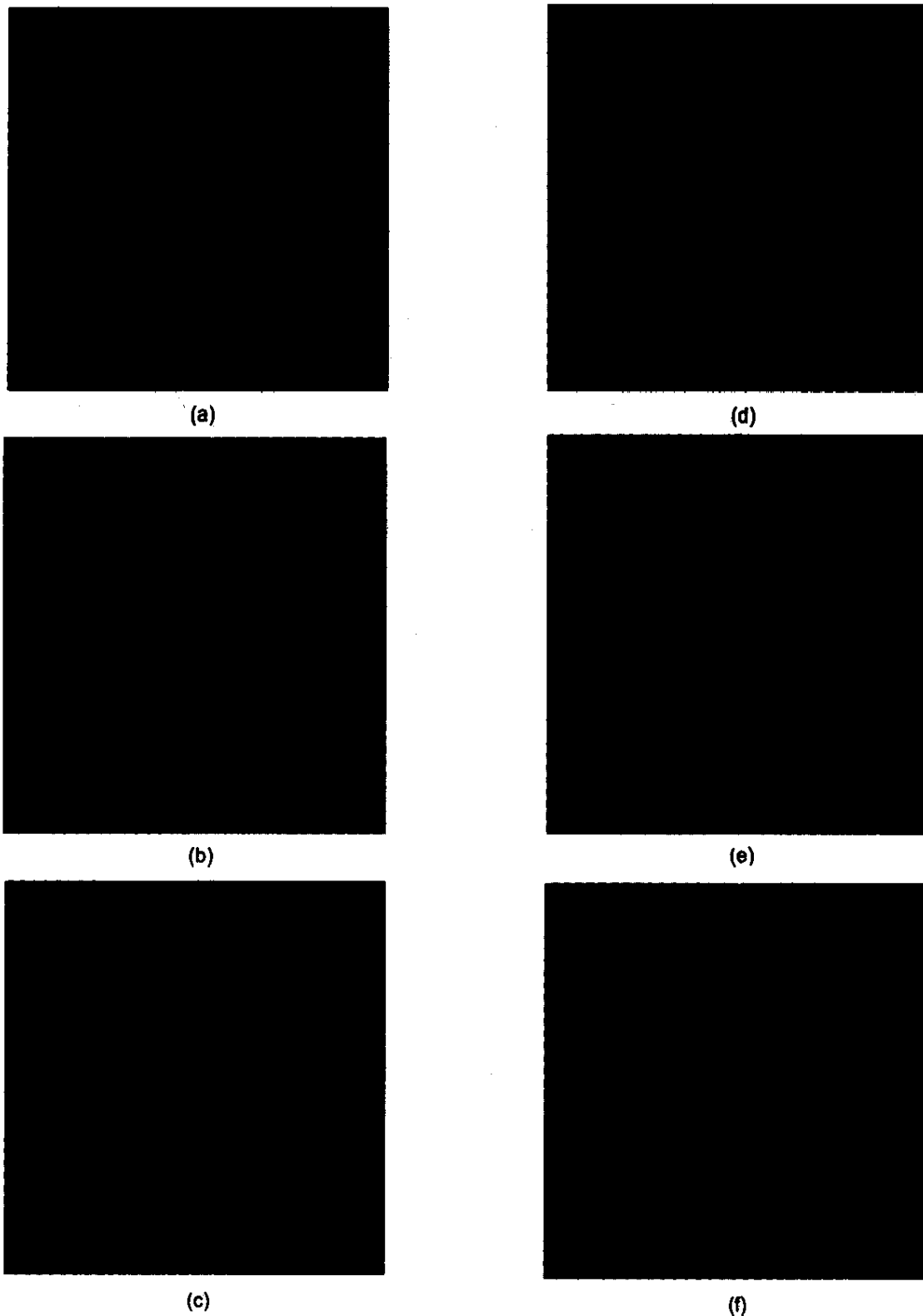


Figure 8. Combined ART-CBP algorithm results with 50 per cent complete symmetric data for 64 rays \times 64 views: (a) original object on 64×64 grid, (b) reconstructed image using CBP, (c) reconstructed image using CBP, (d) reconstructed image with partial data using ART, $\lambda = 0.9$, ART iterations = 80, CPU time = 1.5 min, (e) image after first iteration, $\lambda = 0.9$, ART iterations = 100, CPU time = 2 min, and (f) image after second iteration, $\lambda = 0.9$, ART iterations = 110, CPU time = 2 min.

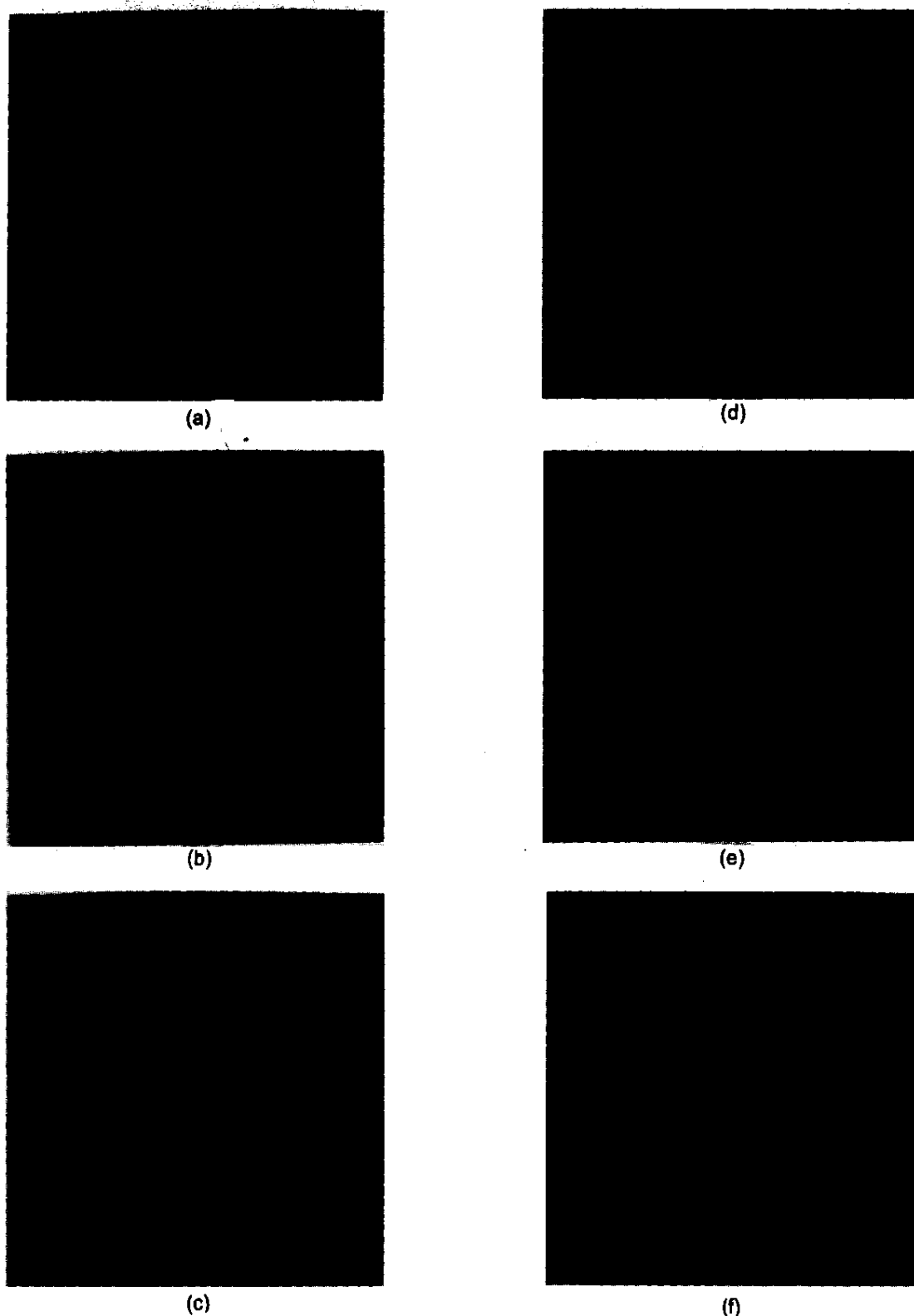


Figure 9. Combined ART-CBP algorithm results with 50 per cent complete symmetric data for 256 rays \times 256 views: (a) original object on 256 \times 256 grid, (b) reconstructed image using CBP, (c) reconstructed image using CBP, (d) reconstructed image with partial data using ART, $\lambda = 0.9$, ART iterations = 18, CPU time = 200 min, (e) image after first iteration, $\lambda = 0.9$, ART iterations = 22, CPU time = 245 min, and (f) image after second iteration, $\lambda = 0.9$, ART iterations = 24, CPU time = 250 min.

There is a significant improvement in the reconstructed images with iterations, but a bright ring appears in the object field. The size of the ring is exactly equal to that of the projection data, namely, 0.75 (Figs 4 to 7) and 0.5 (Figs 8 and 9). It is of one pixel-width. The ring is then to be expected at the interface between the interior recorded projection dataset (that is fixed from one iteration to the next) and the exterior projection dataset that is updated iteratively using CBP.

With iterations, the ring becomes brighter and attains the highest pixel value. The formation of a ring is not a problem since it can be removed at any stage by conventional image processing operations, such as filtering.

The object reconstruction obtained with the 50 per cent projection data has more artifacts and distortions as compared to the 75 per cent data set. The trends in the solution are seen to be similar when the combined ART-CBP algorithm is used. On a conservative side, however, it should be concluded that scanning only 50 per cent of the object in each projection would result in serious artifacts. Thus despite convergence, the solution may not be useful even for a qualitative evaluation.

7. CONCLUSIONS

A novel approach of combining the CBP and the ART to account for incomplete projection data during tomographic inversion has been proposed. The results obtained lead to the following conclusions:

- With the proposed algorithm, the reconstruction with incomplete projection data is qualitatively acceptable. There is a marked improvement in the reconstructed images using the combined ART-CBP algorithm over those obtained using ART alone.
- The artifacts introduced due to incomplete data diminish using ART-CBP algorithm, with increasing iterations. However, a bright ring of one pixel-width appears at the interface

of the original projection data and projection data obtained from reconstructed image.

- Working with less than 50 per cent of the total object size is not recommended for the CT.

ACKNOWLEDGEMENTS

The authors are grateful to Shri Pahlada, Director, Defence Research & Development Laboratory (DRDL), Hyderabad, for the financial support given for this work. Useful discussions with Shri S.B. Kumar and Dr C. Muralidhar are gratefully acknowledged.

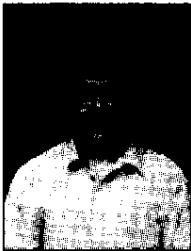
REFERENCES

1. Herman, G.T. *Image reconstruction from projections: The fundamentals of computerised tomography*. Academic Press, New York, 1980.
2. Manzoor, M.F.; Yadav, P.; Muralidhar, K. & Munshi, P. Image reconstruction of simulated specimens using convolution back projection. *Def. Sci. J.*, 2001, **51**(2), 175–87.
3. Myller, M.; Arce, G.R. & Steiner, K.V. Tomographic imaging and synthetic detector arrays. Annual Technical Report, University of Delaware, Centre for Composite Materials, 1993.
4. Ramachandran, G.N. & Lakhshminarayanan, A.V. Three-dimensional reconstruction from radiographs and electron micrographs: Application of convolution instead of Fourier transforms. *Proc. Natl. Sci. Acad. USA*, 1970, **68**, 2236–240.
5. Gordon, R. A tutorial on ART. *IEEE Trans. Nucl. Sci.*, 1974, **21**, 78–93.
6. Mishra, D.; Muralidhar, K. & Munshi, P. A robust MART algorithm for tomographic application. *Numer. Heat Transf.*, 1999, **35**(B), 485–06.
7. Mayinger, F. *Optical measurements: Techniques and applications*. Springer-Verlag, Berlin, 1994.

8. Gordon, R. & Herman, G.T. Three-dimensional reconstruction from projections: A review of algorithm. *Int. Rev. Cytol.*, 1974, **38**, 111-51.
9. Natterer, F. The mathematics of computerised tomography. John Wiley & Sons, New York, 1986.

Contributors

Mr Suneet Singh completed his MTech (Nuclear Engg) from the Indian Institute of Technology (IIT), Kanpur, in 2000. Later, he worked on a DRDL-sponsored project for one year. He is presently a doctoral candidate in Nuclear Engineering at the University of Illinois, at Urbana Champaign, USA.



Dr K Muralidhar obtained his PhD from the University of Delaware, USA, in 1985 and was a postdoctoral fellow at the University of Delaware as well as at the Lawrence Berkeley Laboratory, California, USA, during 1985-87. Presently, he is working as Professor at IIT, Kanpur. He is the recipient of the INSA/JSPS Invitation Fellowship from Japan. He was a Visiting Research Professor at the SUNY Stony Brook, USA. He was awarded the *Institution Prize of Institution of Engineers (India)* for a paper on enhanced oil recovery, and *M.G. Deshpande Best Paper Prize* in the National Fluid Mechanics and Fluid Power Conference. His areas of research include: Optical instrumentation, turbulence measurement, enhanced oil recovery, and cryogenics.



Dr P Munshi obtained his BTech (Mech Engg) from IIT, Kanpur, in 1977; MS (Nuclear Engg) from the Ohio State University, USA, in 1979, and PhD (Nuclear Engg) in 1989 from IIT, Kanpur. Presently, he is Professor at IIT, Kanpur. Before joining IIT, Kanpur, he worked for the Commonwealth Edison Company, USA, for three years as a nuclear thermal safety analysis engineer. His areas of research are: Computerised tomography, nondestructive testing, multiphase flow measurement, fractals, and nuclear reactor safety analysis. He is the recipient of the Alexander von Humboldt Research Fellowship (Fraunhofer-Institute of Nondestructive Testing, Saar-bruecken, Germany), the INSA-DFG Fellowship (University of Hannover, Germany) and the DST-BMBF Indo-German Fellowship. He has been a Visiting Scientist at the London Hospital Medical College. *The American Journal for Mathematical and Management Sciences* awarded him the *Jacob Wolfowitz Prize* (1995) for the outstanding theoretical paper. He received the *Best Paper (R&D) Award in NDE* (2000).